



HAL
open science

DNS and LES of spark ignition with an automotive coil

Olivier Colin, Martin Ritter, Corine Lacour, Karine Truffin, Sophie Mouriaux,
Sergey Stepanyan, Bertrand Lecordier, Pierre Vervisch

► **To cite this version:**

Olivier Colin, Martin Ritter, Corine Lacour, Karine Truffin, Sophie Mouriaux, et al.. DNS and LES of spark ignition with an automotive coil. Proceedings of the Combustion Institute, 2019, 37 (4), pp.4875-4883. 10.1016/j.proci.2018.08.021 . hal-02018875

HAL Id: hal-02018875

<https://hal.science/hal-02018875v1>

Submitted on 14 Feb 2019

HAL is a multi-disciplinary open access archive for the deposit and dissemination of scientific research documents, whether they are published or not. The documents may come from teaching and research institutions in France or abroad, or from public or private research centers.

L'archive ouverte pluridisciplinaire **HAL**, est destinée au dépôt et à la diffusion de documents scientifiques de niveau recherche, publiés ou non, émanant des établissements d'enseignement et de recherche français ou étrangers, des laboratoires publics ou privés.

Manuscript Number:

Title: DNS and LES of spark ignition with an automotive coil

Article Type: 11. Internal Combustion Engines

Keywords: spark ignition; modelling; minimum ignition energy; DNS; LES

Corresponding Author: Dr. Olivier Colin, PhD

Corresponding Author's Institution: IFPEN

First Author: Olivier Colin, PhD

Order of Authors: Olivier Colin, PhD; Martin Ritter, Engineer; Karine Truffin, PhD; Corine Lacour, PhD; Sophie Mouriaux, PhD; Bertrand Lecordier, PhD; Pierre Vervisch, PhD

Abstract: The cycle to cycle combustion variability which is observed in spark-ignition engines is often caused by fluctuations of the early flame development. LES can be exploited for a better understanding and mastering of their origins. For that purpose appropriate models taking into account energy deposition, mixture ignition and transition to propagation are necessary requirements. This paper presents first DNS and LES of spark ignition with a real automotive coil and simplified pin-pin electrodes. The electrical circuit characteristics are provided by ISSIM while the energy deposition is modelled by Lagrangian particles. The ignition model is first evaluated in terms of initial spark radius on a pin-pin ignition experiment in pure air performed at CORIA and EM2C laboratories, showing that it pilots the radius of the torus formed by the initial shock wave. DNS of a quiescent lean propane/air mixture are then performed with this ignition system and a two-step mechanism. The impact of the modelled transferred energy during glow phase as well as the initial arc radius on the minimum ignition energy (MIE) are examined and compared to experimental values. Replacing the two-step chemistry by an analytically reduced mechanism leads to similar MIE but shows a different ignition kernel shape. Finally, LES of turbulent ignition using a Lagrangian arc model show a realistic prediction of the arc shape and its important role on the energy transfer location and thus on the flame kernel shape.

DNS and LES of spark ignition with an automotive coil

Olivier Colin^{a,*}, Martin Ritter^a, Karine Truffin^a, Corine Lacour^b, Sophie Mouriaux^c, Bertrand Lecordier^b, Pierre Vervisch^b

^a*IFPEN, 1 à 4 av. du Bois Préau, 92852 Reuil-Malmaison, France*

^b*CORIA, CNRS, Normandie Univ, INSA, 76801 Saint-Etienne-du-Rouvray, France*

^c*SAFRAN Tech, rue des Jeunes Bois, 78772 Magny-les-Hameaux, France*

Abstract

The cycle to cycle combustion variability which is observed in spark-ignition engines is often caused by fluctuations of the early flame development. LES can be exploited for a better understanding and mastering of their origins. For that purpose appropriate models taking into account energy deposition, mixture ignition and transition to propagation are necessary requirements. This paper presents first DNS and LES of spark ignition with a real automotive coil and simplified pin-pin electrodes. The electrical circuit characteristics are provided by ISSIM while the energy deposition is modelled by Lagrangian particles. The ignition model is first evaluated in terms of initial spark radius on a pin-pin ignition experiment in pure air performed at CORIA and EM2C laboratories, showing that it pilots the radius of the torus formed by the initial shock wave. DNS of a quiescent lean propane/air mixture are then performed with this ignition system and a two-step mechanism. The impact of the modelled transferred energy during glow phase as well as the initial arc radius on the minimum ignition energy (MIE) are examined

*Corresponding author

Email address: `olivier.colin@ifpen.fr` (Olivier Colin)

and compared to experimental values. Replacing the two-step chemistry by an analytically reduced mechanism leads to similar MIE but shows a different ignition kernel shape. Finally, LES of turbulent ignition using a Lagrangian arc model show a realistic prediction of the arc shape and its important role on the energy transfer location and thus on the flame kernel shape.

Keywords: spark ignition, modelling, minimum ignition energy, DNS, LES

1. Introduction

To reduce the fuel consumption of spark ignition (SI) engines, current technologies aim at using a high dilution ratio or a very lean mixture. In both cases, it was shown [1] that this leads to increased cycle to cycle variabilities which are largely caused by fluctuations of the early flame development. Increasing the spark plug energy reduces this initial variability [1] but only to a certain extent. There is therefore a need to better understand and potentially improve spark ignition in such conditions. For this purpose, LES appears as an appropriate tool. Most LES spark ignition models [2] provide a global representation of ignition which is sufficient to study cycle to cycle variability in standard conditions but not when ignition becomes difficult. In this case, accurate models including energy deposition, mixture ignition and transition to propagation are required. Appart from first attempts in LES [3], most studies are performed with DNS like the one of Kravchik et al [4] who performed 2D cylindrical DNS with reduced mechanism for methane and plasma. He evidenced the importance of the initial shock wave on ignition and studied the influence of the deposited energy, initial channel and electrodes diameters. Similarly H₂/air [5] and pure air [6] ignition DNS where succesfully

compared to experimental Schlieren and temperature. While these studies dealt with short duration sparks not representative of an automotive spark plug, Ishii [7] performed similar simulations for propane/air with one-step chemistry, but including a simplified breakdown and glow phase.

In this study, we propose to characterize the energy deposition of a real automotive coil and to figure out if it is possible to recover the experimental minimum ignition energy (MIE), an essential quantity for ignition modelling. Section 2 presents the electrical circuit model and the energy deposition model by Lagrangian particles. The ignition model is first evaluated in Section 3 on a pin-pin ignition experiment in pure air performed at CORIA and EM2C laboratories. Then quiescent DNS of a lean propane/air ignition of the same experiment are presented in Section 4 with a focus on the MIE. Finally, Section 5 presents a first LES of a turbulent propane/air ignition experiment using the same ignition system.

2. Spark plug model

2.1. Electrical circuit model

Although an automotive coil is complex in terms of electronic components it can be globally considered as an inductive system as described in the ignition model ISSIM [2]. In the CORIA experiment, the primary energy E_p of an Audi coil was experimentally evaluated measuring current and voltage as a function of the dwell time t_d (time given for charging the primary inductance), varying between 0.5 and 4 ms. The following quadratic function was proposed: $E_p = 14.5t_d + 15t_d^2$. At spark timing, the energy E_p is transferred to the secondary circuit of the coil with an efficiency η_p .

Based on calorimetric measurements performed at Continental [8], a value of 0.6 was found, in good agreement with previous holographic thermometry measurements [9]. The initial secondary energy $E_s^0 = \eta_p E_p$ is then known (see Fig.S1 in Supplementary Material).

The spark starts with the breakdown phase [10] which consumes an energy E_{bd} from E_s^0 . Measurements performed at CORIA [11] showed that this energy corresponded to the one stored in a capacitance C of 11 pF, giving $E_{bd} = \frac{1}{2} C U_{bd}^2$. It was found that breakdown voltage U_{bd} increases with t_d and with the fuel/air equivalence ratio Φ . Two experimental correlations for U_{bd} were used in the DNS (Fig.S1): one for air and the other for $\Phi > 0.5$, for t_d going from 0.5 and 4ms. It was indeed observed that voltage and current measurements hardly varied for $0.5 < \Phi < 1.5$. In the following glow phase, the secondary energy is given [2] by $dE_s/dt = -U_{spk} I_s - R_s I_s^2$ where U_{spk} , I_s and R_s are the inter-electrode voltage, secondary circuit current and resistance. I_s is given by $I_s = \sqrt{2E_s/L_s}$ where L_s is the secondary circuit inductance. U_{spk} can be decomposed into gas column U_{gc} plus anode and cathode fall voltages U_c and U_a , here taken equal to those of steel (252 V and 18 V). U_{gc} is finally given by the empirical formula from Pashley et al. [12]: $U_{gc} = C_1^U 396.10^3 l_{spark} (10^{-5} P)^{0.182} / (10^3 I_s)^{0.414 C_2^U}$, where l_{spark} is the spark length, P the pressure and I_s the secondary current. The unknown parameters L_s , R_s , C_1^U and C_2^U , given in Table S1, were adjusted using measurements of U_{spk} and I_s during the glow phase at $\Phi = 0.75$, both for quiescent and turbulent conditions. As seen in Fig. 1, the evolution of U_{spk} and I_s , as well as the spark duration, are well reproduced for two dwell times. The progressive rise of U_{spk} also matches the experiment thanks to

U_{gc} correlation which is inversely proportional to I_s .

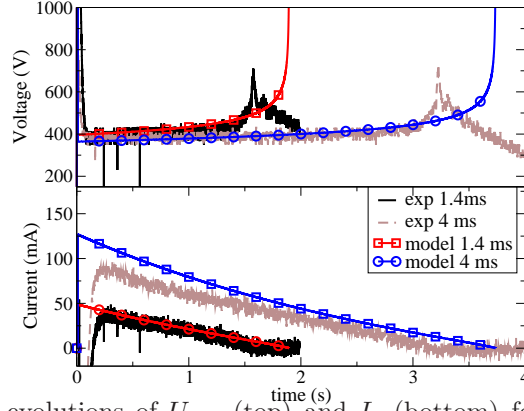


Figure 1: Temporal evolutions of U_{spk} (top) and I_s (bottom) for the condition 1 bar, 300K, $\Phi = 0.75$ and two dwell times of 1.4 and 4 ms.

2.2. Energy transfer to the gas

The electrical power effectively transferred to the gas can now be deduced from the electrical circuit model:

$$P_{ign} = \eta_{bd}P_{bd} + \eta_{glow}U_{gc}I_s \quad (1)$$

The breakdown phase efficiency η_{bd} is set to unity in agreement with [10]. P_{bd} is modeled as a constant power supply over a time t_{bd} : $P_{bd} = E_{bd}/t_{bd}$. While t_{bd} is close to 1-10 ns [10], we checked (not shown here) that increasing t_{bd} up to 200 ns leads essentially to the same ignitions because the energy is released at a nearly constant volume. The power $P_{ign}(t)$ must then be distributed spatially on the CFD mesh. For this purpose a set of N Lagrangian particles are initialized between the electrodes at breakdown. Appart for the first and last particules locating the arc extremities, all particles are convected at the local gas velocity \tilde{u} and undergo a molecular diffusion given by the arc

curvature γ and the plasma diffusivity ν_{plasma} :

$$\frac{dx_p}{dt} = \tilde{u}(x_p, t) + \nu_{plasma}\gamma(T_{plasma}, p)\mathbf{n} \quad (2)$$

where x_p is the particle position and n the normal to the arc. ν_{plasma} is tabulated as a function of pressure and plasma temperature [8], estimated here as 3000 K. Due to the arc convection by turbulence, the distance between consecutive particles can become too small or too large. In this case an algorithm suppresses or adds particles when necessary. The total length l_{spark} of the arc is calculated as the sum of the distances between consecutive particles. In order to distribute $P_{ign}(t)$ along the arc, we define the minimum distance between any node “i” and the arc as $R_i = \min_k(|x_i - x_{pk}|)$, which allows to define a weighting factor $w_i = 0.5(1 + \tanh(3(1 - R_i/r_{arc})))$ where r_{arc} is the initial arc radius that needs to be defined. The power P_i received by node i finally reads $P_i = \frac{w_i}{\int_i w_i dV_i} P_{ign}$. Note that in a case without convection, P_i gives a cylindrical profile of radius r_{arc} .

3. DNS of spark in air

3.1. Numerical set-up

In this section we consider the case $\Phi = 0$ and $t_d = 4$ ms, for a first evaluation of the spark plug model. Calculations are performed on a tetrahedral mesh of 178000 nodes with AVBP [13], a parallel explicit and compressible LES/DNS solver, using the centered second order Lax-Wendroff scheme for convection. As seen in Fig.2 only the extremity of the pin-pin geometry is meshed as the study is limited to short ignition times. The cell size is approximately $50 \mu m$ in the vicinity of the electrodes and becomes much

larger 2mm away. The domain is a sphere of 2cm radius with electrodes located at the center. A non reflecting NSCBC condition with relaxation on pressure is used on the sphere. On the electrodes an isothermal no slip wall law condition is used [14] with $T_w = 300$ K. As seen in Fig. 3, the

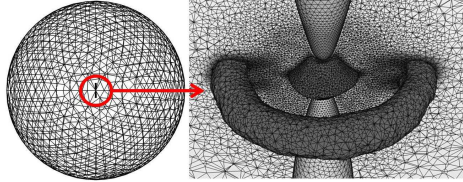


Figure 2: Left: global view of the mesh. Right: 2D slice of the mesh and 3D iso-surface of temperature at 1500K showing the hot gases (torus and inter-electrode zone). Time $t=200 \mu s$.

secondary energy E_s goes from $E_s^0 = 179$ mJ to zero. It is distributed between Joule losses $E_{Joule} = \int_t R_s I_s dt$ (109 mJ), cathode and anode fall losses $E_{falls} = \int_t (U_c + U_a) I_s dt$ (50 mJ), and gas column energy E_{gc} (20mJ). E_{gc} is itself the sum of the initial breakdown energy E_{bd} (0.9mJ) and glow energy $E_{glow} = \int_t U_{gc} I_s dt$ (19.1mJ). This gives a glow phase efficiency, defined as $E_{glow} / (E_{falls} + E_{glow})$, of 0.28, in good agreement with previous studies [4, 10]. The ignition energy, Eq. (1), is finally given by $E_{ign} = \eta_{bd} E_{bd} + \eta_{glow} E_{gc}$ ($\eta_{glow}=0.5$ in Fig. 3).

3.2. Determination of the arc radius r_{arc}

With the previously adjusted electrical circuit model, only two parameters remain to be defined: the radius r_{arc} and the efficiency η_{glow} . The breakdown phase leads to the formation of a shock wave as seen in Fig. 4 showing Schlieren images from EM2C and density from the DNS. The shock radius evolution is found in good agreement with the experiment as confirmed in

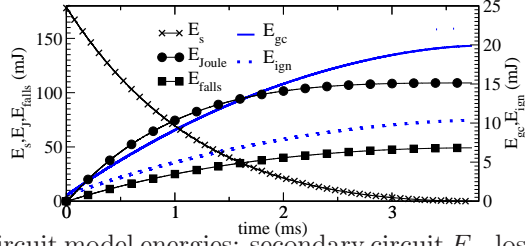


Figure 3: Electrical circuit model energies: secondary circuit E_s , lost by Joule effect E_{Joule} , lost at anode and cathode fall E_{falls} , transferred to the gas column E_{gc} and available for ignition E_{ign} , for case $\Phi = 0$, 1 bar, 300 K.

Fig. 5 left. It can be observed that the two DNS with $r_{arc} = 0.3$ or 0.4 mm lead to very similar shock radius although the initial peak pressure (11.5 and 6.3 bars respectively at around 250ns) are very different. This indicates

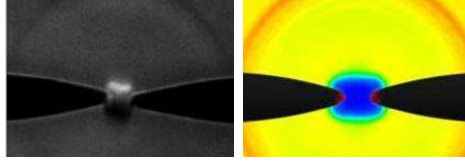


Figure 4: Experimental Schlieren (left) and DNS density (right) of spark in air at $6 \mu s$. distance between electrodes: 0.8 mm.

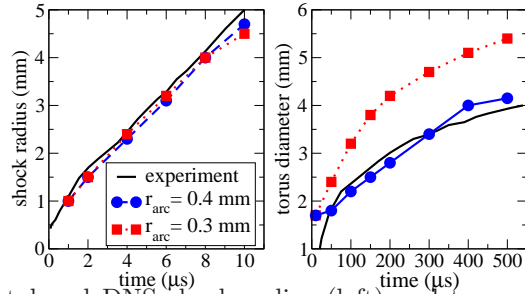


Figure 5: Experimental and DNS shock radius (left) and torus diameter (right) versus time.

that the shock cannot be used to evaluate r_{arc} . But this shock produces an air entrainment along the electrodes which creates a torus as seen in Fig. 2 right and in experiments [15]. Fig. 5 right shows the evolution of the torus

diameter for the EM2C experiment and for the two DNS. It can be observed that the initial radius is similar for both simulations, but the 0.3 mm case leads to a faster torus development which is explained by the larger initial pressure rise. Based on this comparison we chose $r_{arc} = 0.4$ mm as a reference value for quiescent ignitions.

3.3. Evaluation of the glow efficiency η_{glow}

During the glow phase, only a very small fraction of energy is lost by radiation [10], we should therefore expect η_{glow} to be close to unity in Eq. (1). In order to evaluate η_{glow} we compare in Fig. 6 the DNS temperature with that obtained by SRS (Spontaneous Raman Scattering) [11]. The experimental window is reproduced in the DNS visualizations with identical color scale. With $\eta_{glow}=1$ (not shown), the DNS strongly overpredicts the temperature. This could be explained by i/the absence of plasma physics and air dissociation models, ii/an under-prediction of the mixing between fresh and hot gases, iii/an under-prediction of the plasma heat losses at walls. With $\eta_{glow}=0.5$, a correct match is obtained in terms of shape while temperature is still slightly over-predicted. $\eta_{glow}=0.25$ gives lower temperatures, but on a too confined zone. As η_{glow} remains uncertain, its influence will be investigated in the following propane/air ignitions.

4. DNS of quiescent propane/air spark ignition

Quiescent propane/air ignitions were performed at CORIA and showed that minimum dwell time (MDT), defined as the one allowing 100 % ignition, remains close to 0.75ms for Φ larger than 0.8, then rapidly increases for leaner mixtures up to 2.5ms (see Fig. S2), corresponding to $E_s^0 = 78$ mJ, at

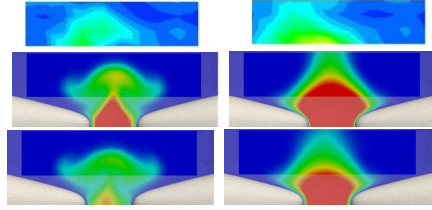


Figure 6: Temperature fields at 0.1 and 1 ms for ignition in air and $t_d = 4$ ms. Top row: experiment, middle and bottom rows: DNS with $\eta_{glow} = 0.5$ and 0.25 . Blue: 300K, red: 1800K.

$\Phi = 0.65$. The first regime corresponds to fast ignitions where the energy brought by the breakdown phase is sufficient. The second regime in which the glow phase energy is necessary to ignite the mixture, corresponds to slow ignitions like encountered in SI engines operating with very lean or diluted mixtures. The case $\Phi = 0.65$ is considered here for this reason. The present DNS were performed with the same mesh and numerical parameters as in the pure air case. For chemistry, the Schmidt and Prandtl numbers were set equal to those found in the burned gases at equilibrium (see Table S2). A two-step mechanism for propane/air was used. Its parameters shown in Table S3, were adjusted to recover a correct laminar flame speed S_l of 0.17 m/s at $\Phi = 0.65$, as measured in [16]. Table 1 presents the DNS cases performed. For each case, the MDT was looked for, by steps of 0.5ms. This MDT corresponds to a minimum value of E_s^0 , which we define as the MIE. For case A, the parameters were chosen based on the previous DNS in air. A MIE of 107 mJ was found, in correct agreement with the experiment (78 mJ). Decreasing η_{glow} to 0.25 systematically leads to extinction, even with the largest dwell time. Increasing η_{glow} from 0.5 to 0.75 (case B) leads to a moderately reduced MIE of 78 mJ, indicating that even if η_{glow} is uncertain, a reasonable MIE is

recovered. Decreasing r_{arc} from 0.4 to 0.3 mm (case C) does not modify the MIE, as found in previous studies [6, 17]. This result is also encouraging for modelling because r_{arc} is difficult to evaluate in practical cases. Cases Aarc and Barc are identical to A and B but the two-step mechanism is replaced by an analytically reduced mechanism based on [18] using the YARC reduction tool [19]. This mechanism includes 21 species, 316 reactions and 12 QSS species. For $\eta_{glow} = 0.5$, case Aarc, ignition was not possible at 107 mJ, while for $\eta_{glow} = 0.75$, case Barc, a MIE of 78 mJ was recovered like for case B. This result shows that globally the reduced mechanism predicts similar MDT as the two-step, although it requires a larger energy in the glow phase, as seen in [17].

Quantity	A	B	C	Aarc	Barc
r_{arc} (mm)	0.4	0.4	0.3	0.4	0.4
$\eta_{glow}(-)$	0.5	0.75	0.5	0.5	0.75
MIE (mJ)	107	78	107	>107	78

Table 1: Propane/air DNS parameters.

Fig. 7 shows for each case the total heat release rate (HRR) for two simulations: one at the MIE and one just below it. For instance A-107mJ corresponds to case A with $E_s^0 = 107$ mJ, leading to ignition, and A-78mJ to case A with $E_s^0 = 78$ mJ, leading to extinction. The propane mass fraction on a 2D plane crossing the electrodes is presented in Fig. 8 for cases A-107mJ and A-78mJ and in Fig. 9 for cases Barc-78mJ and Barc-53mJ. The initial peak of HRR observed in Fig. 7 for A cases before 0.1 ms corresponds mostly to the auto-ignition of the heated mixture located between the electrodes. After this peak a premixed flame starts propagating both between the electrodes

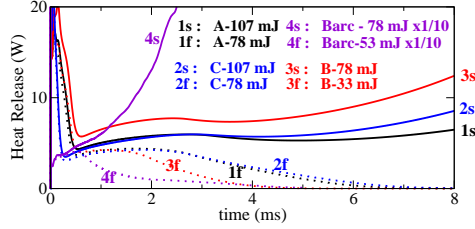


Figure 7: Total heat release rate (W) for the quiescent pin-pin case.

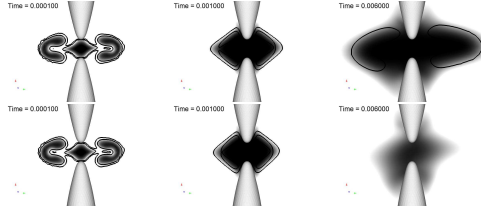


Figure 8: Propane mass fraction and HRR iso-surfaces for cases A-107mJ (top) and A-78mJ (bottom), at 0.1, 1 and 6 ms. Black: $Y_F = 0$, white: $Y_F = 0.037$.

and on the torus as seen at 0.1 ms in Fig. 8. The rapid decrease of the HRR up to 0.5 ms is then explained by the extinction of the torus. The total HRR then slowly increases up to 2 ms approximately in both simulations. Afterwards, case A-107mJ presents a plateau up to around 5 ms followed by a slow rise of the HRR corresponding to a nearly spherical flame expansion. Case A-78mJ on the contrary presents a decrease to zero corresponding to a thickening and shrinking reaction zone. While cases B and C are qualitatively identical to case A, Barc simulations show a very different ignition: up to 0.5 ms, the HRR is approximately 10 times larger for both Barc-78mJ and Barc-53mJ compared to case A, indicating a much intense combustion in the torus. After this instant, the flame grows rapidly in the torus region for Barc-78mJ, which explains the very rapid flame growth compared to case A. On the contrary, extinction is observed on the torus of Barc-53mJ at 1.5 ms, a complete extinction in the inter-electrodes region at 5 ms.

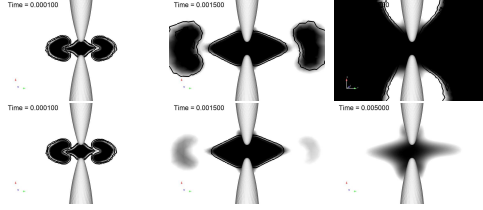


Figure 9: Propane mass fraction and HRR iso-surfaces for cases Barc-78mJ (top) and Barc-53mJ (bottom), at 0.1, 1.5 and 5 ms. Black: $Y_F = 0$, white: $Y_F = 0.037$.

5. LES of turbulent propane/air spark ignition

5.1. LES in air

In the turbulent CORIA experiment [20], Fig. 10, the propane/air mixture is pushed in a rectangular chamber of size 6x6x10cm by a one-stroke piston which position is recorded in time (see Fig.S3). Motion starts at $t=0$ and ends at $t=80\text{ms}$, leading to a final pressure of 2.8 bar (see Fig.S3) and a temperature around 380K. The mixture enters the chamber by a slot with an angle of 65° to the vertical thus allowing a tumble motion reminiscent of a SI engine. The same pin-pin spark plug as in the quiescent experiment is mounted in the chamber as shown in Fig. 10. LES are performed with AVBP using the same moving mesh methodology as for piston engines and around 1.2 million nodes. Smagorinsky turbulent viscosity model is used and walls are assumed isothermal at 300 K.

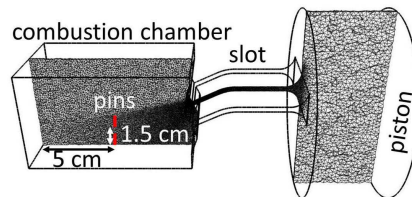


Figure 10: Experimental setup and view of the LES mesh.

First, experiments were performed with air without spark to measure the velocity field by PIV. Good agreement is found between instantaneous LES and experimental velocities as seen in Fig. 11, left. At 20 ms, the inclined jet creates a tumble motion that develops in the whole chamber. At 80 ms the piston stops, no more air enters the chamber and the tumble motion slows down. These experiments were repeated with ignition in air at $t=90$ ms to

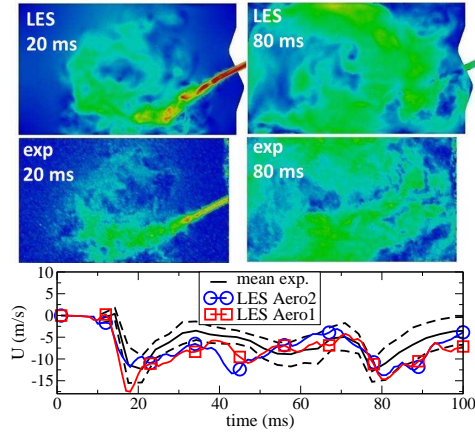


Figure 11: Experimental and LES (Aero1) velocity fields on the mid-plane at 20 and 80 ms (top); blue: 0 m/s, Red=35 m/s. X-axis velocity component (m/s) at the spark plug for experiment, LES Aero1 and Aero2 (bottom).

visualize the spark. Two LES were obtained by injecting different random velocity perturbations in the chamber at $t=0$ ms, leading to different velocity fields at the spark plug as seen in Fig. 11, right. Images of the spark for two selected (out of 20) experimental ignitions and the two LES are shown in Fig. 12. It can be seen that LES spark shows a shape similar to the experimental one: for case Aero1, the flow is mainly horizontal, leading to a mushroom like shape, while for Aero2, a strong vertical downward component leads to the downward shift of the arc. Note that the arc in LES is anchored

at the two pin extremities leading to an important contact between the arc and the pin surface for case aero2, while in the experiment, the contact point moves downward along the pin. Future modelling should therefore allow the arc extremity to slide on the electrode surface.

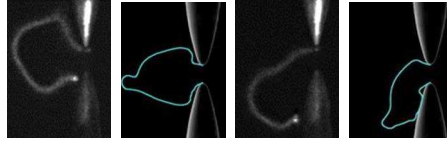


Figure 12: Experimental and LES sparks visualizations (left: Aero1, right: Aero2) 400 μs after spark timing.

5.2. LES of ignition at $\Phi = 0.57$

Like for the quiescent condition, the MDT was obtained experimentally for different fuel/air ratios. Again we choose here the leanest mixture at $\Phi = 0.57$ leading to the longest MDT of 2 ms. The LES velocity field obtained from case Aero1 in Section 5.1 at 90 ms, that is at spark timing (ST), only changing the species mass fractions. This initial solution is interpolated on a mesh of 3 million nodes with a characteristic cell size of 30 microns in the electrodes region, which allows to resolve the flame front thickness of 0.3 mm. The same 2-step mechanism is used with adjusted parameters (see table S4) to recover a laminar flame speed of 0.13 m/s as given by Sandiego mechanism [18]. We chose here a dwell time of 2.5 ms, that is just above the MDT. As the torr radius was not measured in this case, we chose $r_{arc} = 0.2\text{mm}$ corresponding to the same energy density at breakdown as in the quiescent case.

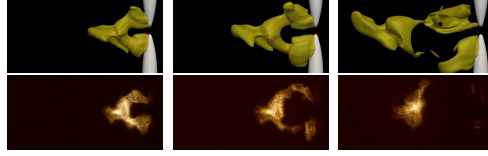


Figure 13: Flame visualisation at times 350, 650 and 1050 μs after ST for the LES (top) and experiment (bottom).

Fig. 13 shows the LES 1000 K iso-surface and the spark along with experimental images of a selected realization. At 350 and 650 μs after ST, the flame is progressively elongated by the strong velocity field generated by the jet. It presents a V-shaped surrounding the spark and attached to the electrodes. Three distinct flame kernels can be seen at 1050 μs , after the end of the spark occurring at 700 μs : two located in the wakes of the electrodes and the third located most downstream on the left, in which combustion is self-sustained. The arms of the V-shaped flame are much thinner indicating that in this region combustion cannot be sustained without the arc. These observations are in good qualitative agreement with the experimental images at the same instants, indicating the correct reproduction of velocity, energy deposition and chemical reactions.

6. Conclusion

First DNS and LES of spark ignition with an automotive coil and simplified pin-pin electrodes were presented. It is first shown that the ISSIM electrical circuit model correctly reproduces experimental voltage and current provided main circuit parameters are experimentally characterized. DNS of spark in air show that the initial spark radius, and thus the initial pres-

sure rise, pilots the radius of the torus formed by the initial shock wave. Comparison with experimental temperature show that the modeled energy transfer to the gas might be overpredicted in the glow phase, requiring an efficiency η_{glow} of 0.5. DNS of a quiescent lean propane/air mixture are then performed with this ignition system and a simplified two-step mechanism. The experimental MIE is correctly recovered for η_{glow} between 0.5 and 0.75, indicating that although not accurate, the modeled transferred energy and the simplified spark description ignoring plasma physics provide acceptable results. Sensitivity to the initial arc radius is on the contrary found weak. Replacing the simplified chemistry by a reduced mechanism leads to similar MIE but shows a different ignition kernel shape. First LES of turbulent ignition using a Lagrangian arc model show a realistic prediction of the arc shape and its role on the energy transfer location and thus on the flame kernel shape.

Acknowledgments

This study was founded by the French ANR research projet FAMAC (ANR-12-VPTT-0002-01). This project was granted access to the HPC resources of CINES and TGCC (no. B06672) from the GENCI eDARI program.

References

- [1] G. Pilla, L. Francqueville, SAE paper 7 (4) (2014) 1734–1743.
- [2] O. Colin, K. Truffin, Proc. Comb. Inst. 33 (2) (2011) 3097 – 3104.

- [3] M. Boileau, G. Staffelbach, B. Cuenot, T. Poinsot, C. Berat, *Combust. Flame* 154 (1-2) (2008) 2 – 22.
- [4] T. Kravchick, E. Sher, J. Heywood, *Combust. Sci. Tech.* 108 (1-3) (1995) 1–30.
- [5] S. Bane, J. Ziegler, J. Shepherd, *Combust. Flame* 162 (2) (2015) 462 – 469.
- [6] B. Sforzo, A. Lambert, J. Kim, J. Jagoda, S. Menon, J. Seitzman, *Combust. Flame* 162 (1) (2015) 181 – 190.
- [7] K. Ishii, T. Tsukamoto, Y. Ujiie, M. Kono, *Combust. Flame* 91 (2) (1992) 153 – 164.
- [8] M. Benmouffok, Ph.D. thesis, INPT (2016).
- [9] D. Verhoeven, *Oil & Gas Sc. and Tech.* 52 (4) (1997) 453–464.
- [10] R. Maly, M. Vogel, *Proc. Comb. Inst.* 17 (1) (1979) 821 – 831.
- [11] C. Lacour, A. Lo, J. Marrero, F. Lefebvre, P. Vervisch, A. Cessou, B. Lecordier, in: *18th Int. Symp. Appl. Laser and Imag. Tech.*, 2016.
- [12] N. Pashley, R. Stone, G. Roberts, in: *SAE World Congress*, 2000.
- [13] T. Schoenfeld, M. Rudgyard, *27th AIAA Conf.* (1999) 1378–1385.
- [14] E. Nicoud, O. Colin, C. Angelberger, F. Nicollet, C. Kruger, submitted to *Oil and Gas Sci. Tech.*

[15] I. Mulla, S. R. Chakravarthy, N. Swaminathan, R. Balachandran, *Combust. Flame* 164 (2016) 303 – 318.

[16] C. Vagelopoulos, F. Egolfopoulos, C. Law, *Proc. Comb. Inst.* 25 (1) (1994) 1341 – 1347.

[17] S. Mouriaux, Ph.D. thesis, Ecole Centrale Paris (2016).

[18] J. Prince, C. Treviao, F. Williams, *Combust. Flame* 175 (Supplement C) (2017) 27 – 33.

[19] P. Pepiot, Ph.D. thesis, Stanford University (2008).

[20] C. Lacour, A. Cessou, B. Lecordier, in: *Europ. Comb. Meeting*, 2013.

List of Figures

1	Temporal evolutions of U_{spk} (top) and I_s (bottom) for the condition 1 bar, 300K, $\Phi = 0.75$ and two dwell times of 1.4 and 4 ms.	5
2	Left: global view of the mesh. Right: 2D slice of the mesh and 3D iso-surface of temperature at 1500K showing the hot gases (torus and inter-electrode zone). Time $t=200 \mu s$	7
3	Electrical circuit model energies: secondary circuit E_s , lost by Joule effect E_{Joule} , lost at anode and cathode fall E_{falls} , transferred to the gas column E_{gc} and available for ignition E_{ign} , for case $\Phi = 0$, 1 bar, 300 K.	8
4	Experimental Schlieren (left) and DNS density (right) of spark in air at $6 \mu s$. distance between electrodes: 0.8 mm.	8

5	Experimental and DNS shock radius (left) and torus diameter (right) versus time.	8
6	Temperature fields at 0.1 and 1 ms for ignition in air and $t_d = 4$ ms. Top row: experiment, middle and bottom rows: DNS with $\eta_{glow} = 0.5$ and 0.25 . Blue: 300K, red: 1800K. . . .	10
7	Total heat release rate (W) for the quiescent pin-pin case. . .	12
8	Propane mass fraction and HRR iso-surfaces for cases A-107mJ (top) and A-78mJ (bottom), at 0.1, 1 and 6 ms. Black: $Y_F = 0$, white: $Y_F = 0.037$	13
9	Propane mass fraction and HRR iso-surfaces for cases Barc-78mJ (top) and Barc-53mJ (bottom), at 0.1, 1.5 and 5 ms. Black: $Y_F = 0$, white: $Y_F = 0.037$	13
10	Experimental setup and view of the LES mesh.	14
11	Experimental and LES (Aero1) velocity fields on the mid-plane at 20 and 80 ms (top); blue: 0 m/s, Red=35 m/s. X-axis velocity component (m/s) at the spark plug for experiment, LES Aero1 and Aero2 (bottom).	14
12	Experimental and LES sparks visualizations (left: Aero1, right: Aero2) 400 μs after spark timing.	15
13	Flame visualisation at times 350, 650 and 1050 μs after ST for the LES (top) and experiment (bottom).	16

Supplementary Material

Document supplementary_material_Colin_et_al.pdf provides figures S1 to S3 and Table S1 to S4.

Fig.S1: Secondary energy E_s^0 and breakdown voltage U_{bd} as a function of dwell time t_d for $\Phi=0$ and 0.5.

Fig.S2: Experimental minimum dwell time (MDT) to ignite a quiescent mixture at $p=1\text{bar}$, $T=300\text{K}$ as a function of Φ . Red: 100 % ignition, black: 0 % ignition.

Fig.S3: Piston position versus time (left ordinate). Experimental and LES pressure in the chamber (right ordinate).

Tab.S1: Choice of modelling constants for voltage U_s at different conditions.

Tab.S2: Schmidt and Prandtl numbers for the case $\Phi = 0.65$, $p=1\text{bar}$ and $T=300\text{K}$.

Tab.S3: Arrhenius constants for the case $\Phi = 0.65$, $p=1\text{bar}$ and $T=300\text{K}$.

Tab.S4: Schmidt and Prandtl numbers for the case $\Phi = 0.57$, $p=2.8\text{bar}$ and $T=380\text{K}$.

Supplemental Material

[Click here to download Supplemental Material: supplementary_material_Colin_et_al.pdf](#)

LaTeX 2 Column File

[Click here to download LaTeX 2 Column File: LaTeX_2_Column_File.pdf](#)